Numerical modelling of a transient conductive-radiative thermal problem arising in silicon purification ⋆

A. Bermúdez [a], R. Leira [a], M.C. Muñiz [a,*], F. Pena [a]

[a] *Department of Applied Mathematics, University of Santiago de Compostela, 15706 Santiago, Spain*

Abstract

The objective of this work is to present and numerically solve a mathematical model for the thermal behavior of a casting ladle devoted to purification of silicon. A nonlinear and non-local boundary condition is considered for radiative heat transfer in an inner closed cavity of the domain. We also propose a numerical approximation using a finite element method. An iterative algorithm and numerical results are presented.

Key words: phase change, non-local boundary condition, Stefan-Boltzmann radiation condition, axisymmetric enclosure, finite elements, numerical simulation.

1 Introduction

Radiative heat transfer plays a major role in a huge range of engineering applications involving high-temperature processes such as glass manufacturing, industrial furnace design and so on (see [5,9,10]). In many cases numerical simulation provides an insight into the radiative analysis of these complex systems and it promotes improvements of the process optimization.

⋆ This work has been supported by MCYT-FEDER DPI2003-01316 and FERROATLANTICA I+D.

* Department of Applied Mathematics, University of Santiago de Compostela, 15706 Santiago, Spain. Tel.: +34-981-563100 ext. 13354. Fax:+34-981-597054

Email addresses: mabermud@usc.es (A. Bermúdez), rleira@usc.es (R. Leira), mcarmen@usc.es (M.C. Muñiz), fpena@usc.es (F. Pena).

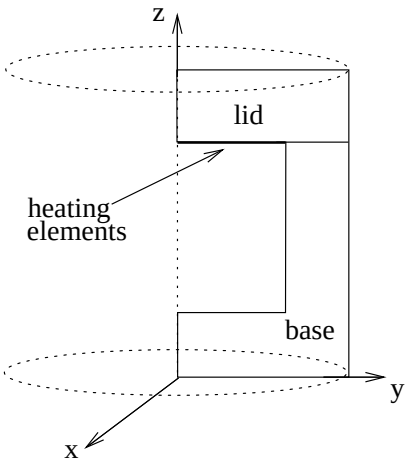

Fig. 1. Meridian section of the ladle without silicon and location of heating elements.

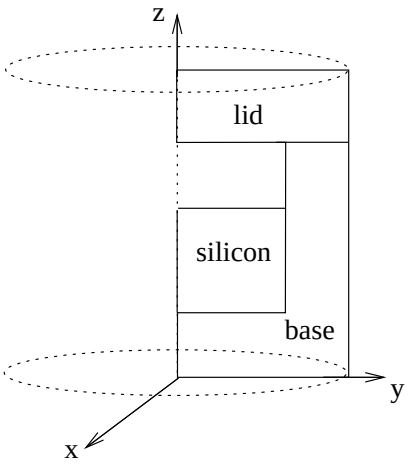

Fig. 2. Meridian section of the ladle with silicon.

The motivation of this work is to compute the numerical solution of the problem addressed in [11] applied to a silicon purification process. Indeed, we present a numerical model describing the thermal behavior of this process which takes place into a so-called *casting ladle*. To the best of the authors knowledge, we present the new contribution of taking into account, simultaneously, the phase change in the silicon and the non-local boundary condition arising from the Stefan-Boltzmann radiation condition at the enclosure surfaces within the ladle.

A related problem where radiative heat transfer plays a major role in the energy balance of the system is the sublimation growth of silicon carbide single crystals (see [3,7]). These papers consider a so-called growth cavity having an axisymmetric geometry which is more general than the inner one in the present paper. Actually, the simplicity of our cavity allows us to compute the radiation kernels in a quite simple way, becoming a challenge for more complicated geometries. However, papers [3,7] do not consider phase transition.

The outline of this article is as follows. In section 2 the physical problem is introduced. In section 3, using the axisymmetry of the domain, we formulate the mathematical problem in a two-dimensional domain by means of cylindrical coordinates. Section 4 is devoted to introduce space and time discretization of the aforementioned problem and to present an iterative algorithm. Finally, in section 5, several numerical results are shown.

2 The physical problem

Metallurgical grade silicon (MG-Si), containing about 1% of other metals, is widely used in the aluminum and silicon chemical industry, the manufacture of semiconductors, solar photo-voltaic cells and so on. It is obtained from a silicon oxide in electrical submerged arc furnaces. A technique of MG-Si purification is to melt it and to induce its directional solidification; this method of removing impurities is based on the fact that most impurities tend to remain in a molten region rather than resolidify.

This purification process is taking place into a casting ladle which consists of a finite axisymmetric cylinder containing a cylindrical enclosure. After the casting ladle being electrically heated, its lid is open and molten silicon is poured into its inner cavity keeping a gap between the top of the silicon and the upper part of the inner ladle surface where several heating elements are located (see figures 1 and 2). The objective is now to push upwards the metal impurities by means of inducing one-directional solidification switching on the heating elements and then keeping molten the top of the silicon ingot. In doing so, the solid silicon grows gradually upwards into the liquid and the metallic impurities are segregated into the melt region during solidification; thus, at the end of the process most of impurities are concentrated at the top of the silicon ingot.

Even though several authors take into account semi-transparency of silicon by considering an additional temperature-dependent term in the thermal conductivity (see [7]), including semi-transparency is out of the scope of this paper. Indeed, radiation heat transfer is considered in the inner cavity and materials of the enclosure are assumed to be opaque (see [6]); therefore radiation may be treated as a surface phenomenon. Moreover, we assume both that the walls of the cylindrical enclosure behave as black surfaces and that the medium within the enclosure is radiatively nonparticipating so that it has no effect on the radiation transfer between inner surfaces. We also assume that radiative properties are independent of wavelength.

3 The mathematical model

In this section we present a thermal model for a transient conductive-radiative heat transfer problem with phase change taking place in the casting ladle. This container is axisymmetric with respect to the $z-$axis and it has an inner cavity, that is to say it is a connected body with disconnected boundary. Using cylindrical coordinates the three-dimensional problem is transformed into a two-dimensional one written on a vertical section of the ladle.

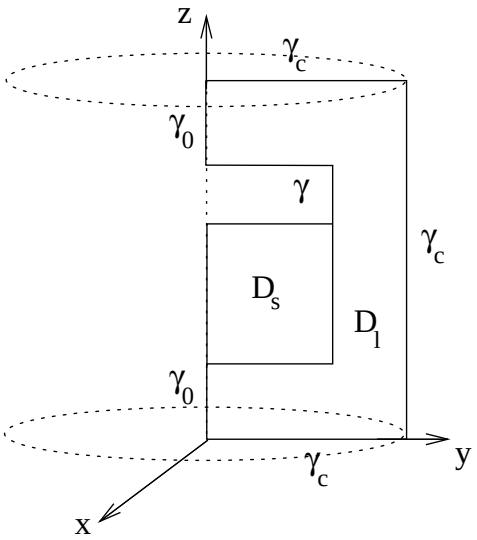

Fig. 3. D: generating surface of Ω.

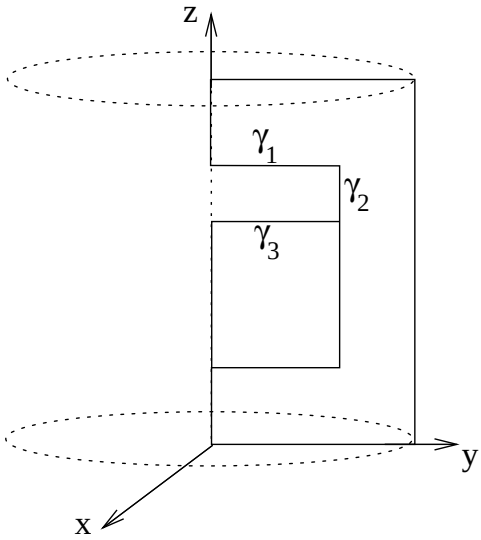

Fig. 4. Subsets of γ.

We denote by $\Omega \subset \mathbb{R}^3$ the casting ladle with silicon, which consists of a domain generated by the rotation about the $z-$axis of a bounded polygonal connected set

$$\mathrm{D} \subset \{(r,z) \in \mathbb{R}^2; r \geq 0\},$$

called meridian section of Ω (see [4]). We assume that Ω has a Lipschitz boundary and that the intersection of the set ∂D with the $z-$axis does not contain isolated points. We assume that the boundary of Ω is the union of two disjoint sets: an outer part, denoted by Γ_c, and an inner boundary, called Γ. Moreover, we assume that the boundary of D is the union of $\overline{\gamma}_0$, $\overline{\gamma}_c$ and $\overline{\gamma}$ where γ_0, γ_c and γ are disjoint open sets and (see figure 3),

- γ_0 is a subset of the $z-$axis,
- γ_c is the outer part of ∂D,
- γ is the boundary generating Γ.

We denote by γ_1, γ_2 and γ_3 the subsets of γ depicted in figure 4; we denote by Γ_1 the subset of Γ which is generated by rotation of set γ_1 about the $z-$axis.

Similarly, let Ω_s and Ω_l be the subsets of Ω corresponding to silicon and ladle which are generated by rotation of sets D_s and D_l, respectively, about the $z-$axis (see figure 3).

Let $[0,\, \mathcal{T}] \subset \mathbb{R}$ be the time interval with $\mathcal{T} > 0$. Moreover we set $Q_{\mathcal{T}} = \Omega \times (0, \mathcal{T})$. Throughout this paper we denote by $T(\mathbf{x}, t)$ the absolute temperature at each point $\mathbf{x} \in \Omega$ and each time $t \in [0, \mathcal{T}]$. Assuming both there is no convection and there is no internal heat source, transient heat conduction is described by

$$\rho(\mathbf{x}, T) c(\mathbf{x}, T) \frac{\partial T}{\partial t}(\mathbf{x}, t) - \nabla.(k(\mathbf{x}, T) \nabla T) = 0 \text{ in } Q_{\mathcal{T}}, \tag{1}$$

where ρ is density, c is specific heat and k is thermal conductivity, all depending on the spatial variable $\mathbf{x}$ and temperature T. We assume that the medium is piecewise homogeneous and nonlinear, therefore

$$\begin{aligned}
\rho(\mathbf{x},T) &= \chi_{\Omega_s}(\mathbf{x})\ \rho_s(T) + \chi_{\Omega_l}(\mathbf{x})\ \rho_l(T),\\
c(\mathbf{x},T) &= \chi_{\Omega_s}(\mathbf{x})\ c_s(T) + \chi_{\Omega_l}(\mathbf{x})\ c_l(T),\\
k(\mathbf{x},T) &= \chi_{\Omega_s}(\mathbf{x})\ k_s(T) + \chi_{\Omega_l}(\mathbf{x})\ k_l(T),
\end{aligned}$$

where χ_A denotes the characteristic function of the set A. We assume that a change of phase is taking place in Ω_s at a single temperature T_s. Thus, introducing an enthalpy function $\mathrm{H}(\mathbf{x},T)$ we have

$$\mathrm{H}(\mathbf{x},T) = \chi_{\Omega_s}(\mathbf{x})\ \mathrm{H}_s(T) + \chi_{\Omega_l}(\mathbf{x})\ \mathrm{H}_l(T) \tag{2}$$

where

$$\mathrm{H}_s(T) = \begin{cases} \Phi_s(T) & T < T_s,\\ [\Phi_s(T_s), \Phi_s(T_s) + L\ \rho(T_s)] & T = T_s,\\ \Phi_s(T) + L\ \rho(T_s) & T > T_s, \end{cases} \tag{3}$$

$$\mathrm{H}_l(T) = \Phi_l(T), \tag{4}$$

$\Phi_j(T)$ being the function

$$\Phi_j(T) = \int_0^T \rho_j(\zeta) c_j(\zeta)\ d\zeta, \tag{5}$$

with subscript j being both s or l representing silicon or ladle, respectively, and L being the latent heat per unit mass. Notice that multivalued function (3) is accounting for phase change at temperature T_s in the silicon, whereas enthalpy in (4) is considered in the ladle where there is no phase transition.

Hence the heat transfer equation reads

$$\frac{\partial e}{\partial t}(\mathbf{x},t) - \nabla.(k(\mathbf{x},T)\nabla T) = 0 \text{ in } Q_{\mathcal{T}}, \tag{6}$$

where e denotes enthalpy density which is expressed, in terms of temperature, as follows

$$e(\mathbf{x},t) \in \mathrm{H}(\mathbf{x}, T(\mathbf{x},t)). \tag{7}$$

REMARK 3.1 If $\rho_j(T)$ and $c_j(T)$, for $j = s, l$, are continuous functions such that there exist constants $\rho_\star$, $\rho^\star$, $c_\star$ and $c^\star$ for which

$$0 < \rho_\star \leq \rho_j(T) \leq \rho^\star, \quad \forall T \in \mathbb{R}, \quad j = s, l,$$

$$0 < c_\star \leq c_j(T) \leq c^\star, \quad \forall T \in \mathbb{R}, \quad j = s, l,$$

then H is a maximal monotone mapping (see [13]).

3.1 Boundary conditions

On Γ_c a convection boundary condition is considered,

$$k\frac{\partial T}{\partial \mathbf{n}} = \alpha(T_c - T) \text{ on } \Gamma_c, \tag{8}$$

$\mathbf{n}$ being the outward unit normal vector to the boundary, α the convection heat transfer coefficient and T_c the temperature of surroundings.

On Γ_1, subset of the inner boundary Γ, heating elements are considered in order to heat the upper part of the silicon. These thermal devices are switched off if the highest temperature at this boundary, denoted by $\tilde{T}$, is greater or equal than a given temperature $\bar{\theta}$. Thus the boundary condition on Γ is

$$k\frac{\partial T}{\partial \mathbf{n}}(\mathbf{x}) = g(\tilde{T}, t)\, \chi_{\Gamma_1}(\mathbf{x}) + q_{rad}(\mathbf{x}) \text{ on } \Gamma, \tag{9}$$

where

$$\tilde{T}(t) = \max_{\mathbf{x} \in \Gamma_1} T(\mathbf{x}, t). \tag{10}$$

Function g represents the power given to the heating elements and function q_{rad}, which accounts for the radiative contribution, is described below. Let us assume

$$g(T,t) = \begin{cases} p(t) & \text{if } T \leq \underline{\theta}, \\ p(t)(\bar{\theta} - T)/(\bar{\theta} - \underline{\theta}) & \text{if } \underline{\theta} \leq T \leq \bar{\theta}, \\ 0 & \text{if } \bar{\theta} \leq T, \end{cases} \tag{11}$$

where $\underline{\theta}$ is the threshold temperature at which the power begins to decrease and $p(t)$ is a time-dependent function related with the maximum power of the heating device.

The objective of these heating elements located at the upper part of the ladle hole is to keep the top of the silicon molten in order for inducing its directional solidification, i.e., the solid silicon growing upwards into the liquid. Nevertheless, the heating elements have their maximum operating temperature, denoted by $\bar{\theta}$; operation temperatures beyond this threshold value may damage these heating elements so that a thermostat function like (11) is needful to stop the power supply when the threshold value is reached. The system recovers the power supply when the maximum operating temperature on the boundary Γ_1 decreases.

Moreover, on the whole inner boundary Γ we consider a non-local radiative boundary condition assuming that surfaces may be approximated as black surfaces (see [6]). Therefore, energy only leaves the surface as a result of emission and all incident radiation is absorbed. Hence function q_{rad} of (9) is given on Γ by

$$q_{rad}(\mathbf{x}) = J(\mathbf{x}) - R(\mathbf{x}), \tag{12}$$

$J(\mathbf{x})$ and $R(\mathbf{x})$ being the irradiation and the radiosity at point $\mathbf{x}$ of the surface, respectively. Taking into account the Stefan-Boltzmann law and the fact that there is no reflection, radiosity reads

$$R(\mathbf{x}) = \sigma T^4(\mathbf{x}) \text{ on } \Gamma, \tag{13}$$

σ being the Stefan-Boltzmann radiation constant ($\sigma = 5.670 \times 10^{-8} \mathrm{W/m^2\,K^4}$). The irradiation J at a point $\mathbf{x}$ only depends on radiation emitted by the rest of the inner boundary, that is,

$$J(\mathbf{x}) = \int_{\Gamma} F(\mathbf{x}, \mathbf{y}) R(\mathbf{y}) dS_{\mathbf{y}}, \tag{14}$$

where $F(\mathbf{x}, \mathbf{y})$ is the view factor between points $\mathbf{x}$ and $\mathbf{y}$ of Γ, and $dS_{\mathbf{y}}$ is a differential surface element. Thus J and R are related in terms of the integral operator $\mathcal{K}$ defined by

$$\mathcal{K}(\zeta)(\mathbf{x}) = \int_{\Gamma} F(\mathbf{x}, \mathbf{y}) \zeta(\mathbf{y}) dS_{\mathbf{y}}, \quad \mathbf{x} \in \Gamma, \tag{15}$$

therefore (14) reads

$$J(\mathbf{x}) = \mathcal{K}(\sigma T^4)(\mathbf{x}), \tag{16}$$

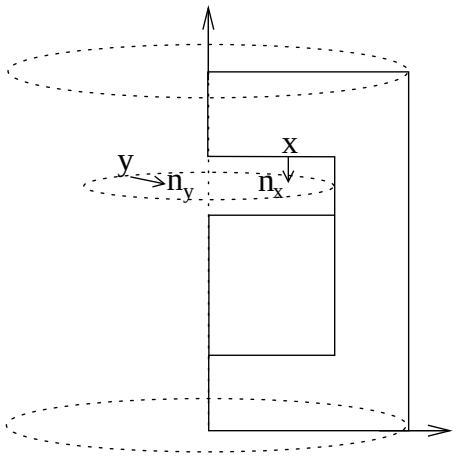

Fig. 5. Normal vectors.

taking into account the Stefan-Boltzmann law. Then using (13) and (16) boundary condition (12) leads to

$$q_{rad}(\mathbf{x}) = \mathcal{K}(\sigma T^4)(\mathbf{x}) - \mathcal{I}(\sigma T^4)(\mathbf{x}) \text{ on } \Gamma, \tag{17}$$

$\mathcal{I}$ being the identity operator.

REMARK 3.2 The view factor between points $\mathbf{x}$ and $\mathbf{y}$ of Γ quantifies the visibility between these two points and it is given by (see [8,11] and references therein)

$$F(\mathbf{x},\mathbf{y}) = \frac{\mathbf{n_x}.(\mathbf{y}-\mathbf{x})\ \mathbf{n_y}.(\mathbf{x}-\mathbf{y})}{\pi\ |\mathbf{x}-\mathbf{y}|^4}, \quad \text{a.e. } (\mathbf{x},\mathbf{y}) \in \Gamma\times\Gamma, \ \ \mathbf{x}\neq\mathbf{y}, \tag{18}$$

$\mathbf{n_x}$ and $\mathbf{n_y}$ being the outward unit normal vectors to Γ at $\mathbf{x}$ and $\mathbf{y}$, respectively, directed outwards Ω (see figure 5). Notice that since the enclosure is a convex set the visibility factor equals one (see [11]).

REMARK 3.3 Since Γ is both a piecewise $C^{1,\delta}$ and a Lipschitz surface with the set of non-smooth points, $\tilde{\Gamma}$, having zero surface measure, the integral

$$\mathcal{K}(1)(\mathbf{x}) = \int_\Gamma F(\mathbf{x},\mathbf{y})dS_\mathbf{y} = 1, \tag{19}$$

for $\mathbf{x}\in\Gamma\backslash\tilde{\Gamma}$ (see [11]).

Taking into account (19) the right hand side of (17) reads

$$\mathcal{K}(\sigma T^4)(\mathbf{x}) - \mathcal{I}(\sigma T^4)(\mathbf{x}) = \int_\Gamma F(\mathbf{x},\mathbf{y})(\sigma T^4(\mathbf{y}) - \ \sigma T^4(\mathbf{x}))dS_\mathbf{y}. \tag{20}$$

Finally (17) leads to

$$q_{rad}(\mathbf{x}) + \mathcal{G}(\sigma T^4)(\mathbf{x}) = 0, \tag{21}$$

where

$$\mathcal{G}(\sigma T^4)(\mathbf{x}) = (\mathcal{I} - \mathcal{K})(\sigma T^4)(\mathbf{x}). \tag{22}$$

On the boundary γ_0 we take into account the axisymmetry of the domain and we have

$$k\frac{\partial T}{\partial \mathbf{n}} = 0 \text{ on } \gamma_0. \tag{23}$$

3.2 Cylindrical coordinates

Due to the axisymmetry of the domain and assuming that all the fields involved in this problem are independent of the angular variable θ, we transform the 3D problem into a 2D one using cylindrical coordinates.

Setting $R_{\mathcal{T}} = \mathrm{D}\times\ (0,\mathcal{T})$, a straightforward computation from (6) and (7) leads to

$$\frac{\partial e}{\partial t} - \frac{1}{r}[\frac{\partial}{\partial r}(rk\frac{\partial T}{\partial r}) + \frac{\partial}{\partial z}(rk\frac{\partial T}{\partial z})] = 0 \text{ in } R_{\mathcal{T}}, \tag{24}$$

$$e(r,z,t) \in H(r,z,T(r,z,t)). \tag{25}$$

On the other hand, if $\mathbf{x} \in \Gamma$, its cylindrical coordinates (r,z,θ) are such that

$$(r,z) \in \gamma, \quad \theta \in [0,2\pi).$$

Since temperature is independent of θ, it reads $T(r,z)$ in cylindrical coordinates and taking $\mathbf{x} = (r,z)$ on γ and $\mathbf{y} = (\tilde{r}\cos\tilde{\theta}, \tilde{r}\sin\tilde{\theta}, \tilde{z})$ on Γ (see figure 5), the heat flux (21) leads to

$$q_{rad}(r,z) = -\mathcal{G}(\sigma T^4)(r,z) = \int_{\gamma} \sigma f(r,z,\tilde{r},\tilde{z})\ [T^4(\tilde{r},\tilde{z}) - T^4(r,z)]\,\tilde{r}\ d\gamma_{(\tilde{r},\tilde{z})}, \tag{26}$$

$d\gamma_{(\tilde{r},\tilde{z})}$ denoting the differential element and f the function accounting for the view factor (18) which reads

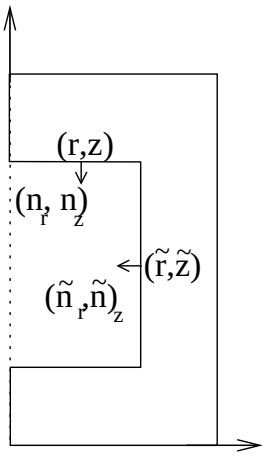

Fig. 6. Normal vectors at inner cavity.

$$f(r,z,\tilde{r},\tilde{z}) = \int_0^{2\pi} \frac{c_2\, cos^2\,\tilde{\theta} + c_1\, cos\,\tilde{\theta} + c_0}{\pi(d - 2r\tilde{r}cos\tilde{\theta})^2} d\tilde{\theta}, \tag{27}$$

where c_0, c_1, c_2 and d are given by

$$\begin{aligned} c_0 &= (-rn_r + n_z(\tilde{z}-z))(-\tilde{r}\tilde{n}_r + \tilde{n}_z(z-\tilde{z})),\\ c_1 &= -(\tilde{r}^2 + r^2)n_r\tilde{n}_r + (z-\tilde{z})(\tilde{r}n_r\tilde{n}_z - rn_z\tilde{n}_r),\\ c_2 &= r\tilde{r}n_r\tilde{n}_r,\\ d &= r^2 + \tilde{r}^2 + (z-\tilde{z})^2, \end{aligned}$$

respectively. Notice that (n_r, n_z) and $(\tilde{n}_r, \tilde{n}_z)$ are the outward unit normal vectors to γ at points (r,z) and $(\tilde{r},\tilde{z})$, respectively (see figure 6). On the other hand, we emphasize the fact that function f is independent of the angular variable θ due to axisymmetry. Moreover, f verifies

$$f(r,z,\tilde{r},\tilde{z}) = f(\tilde{r},\tilde{z},r,z),\ \ \forall (r,z),\ (\tilde{r},\tilde{z}). \tag{28}$$

Remark 3.4 If $r\,\tilde{r} \neq 0$, (27) reads

$$f(r,z,\tilde{r},\tilde{z}) = c_2 \frac{(a_1^3 + a_2^3 - 5a_1a_2^2 - 5a_1^2a_2 + 8a_1^{\frac{3}{2}}a_2^{\frac{3}{2}})}{(a_1-a_2)^2 a_1^{\frac{3}{2}}a_2^{\frac{3}{2}}} + \frac{c_1(a_1-a_2) + c_0(a_1+a_2)}{a_1^{\frac{3}{2}}a_2^{\frac{3}{2}}} \tag{29}$$

where

$$\begin{aligned} a_1 &= (r+\tilde{r})^2 + (z-\tilde{z})^2,\\ a_2 &= (r-\tilde{r})^2 + (z-\tilde{z})^2. \end{aligned}$$

(r,z)	$(\tilde{r},\tilde{z})$	$(n_r,\, n_z)$	$(\tilde{n}_r,\, \tilde{n}_z)$	c_0	c_1	c_2
$\in \gamma_1$	$\in \gamma_1$	$(0,-1)$	$(0,-1)$	0	0	0
$\in \gamma_1$	$\in \gamma_2$	$(0,-1)$	$(-1,0)$	$\tilde{r}(z-\tilde{z})$	$-r(z-\tilde{z})$	0
$\in \gamma_1$	$\in \gamma_3$	$(0,-1)$	$(0,1)$	$(z-\tilde{z})^2$	0	0
$\in \gamma_2$	$\in \gamma_1$	$(-1,0)$	$(0,-1)$	$-r(z-\tilde{z})$	$\tilde{r}(z-\tilde{z})$	0
$\in \gamma_2$	$\in \gamma_2$	$(-1,0)$	$(-1,0)$	$r\tilde{r}$	$-(r^2+\tilde{r}^2)$	$r\tilde{r}$
$\in \gamma_2$	$\in \gamma_3$	$(-1,0)$	$(0,1)$	$r(z-\tilde{z})$	$-\tilde{r}(z-\tilde{z})$	0
$\in \gamma_3$	$\in \gamma_1$	$(0,1)$	$(0,-1)$	$(\tilde{z}-z)^2$	0	0
$\in \gamma_3$	$\in \gamma_2$	$(0,1)$	$(-1,0)$	$-\tilde{r}(z-\tilde{z})$	$r(z-\tilde{z})$	0
$\in \gamma_3$	$\in \gamma_3$	$(0,1)$	$(0,1)$	0	0	0

Table 1. Coefficients of f.

Moreover we obtain

$$f(r,z,\tilde{r},\tilde{z}) = \begin{cases} 2c_0/a_1^2 & \text{if } r\ \tilde{r} = 0, \\ n_r^2/(2\,r^2) & \text{if } (r,z) = (\tilde{r},\tilde{z}),\ r > 0. \end{cases} \tag{30}$$

REMARK 3.5 The values of coefficients of function f are given in table 1 by taking into account the shape of the inner boundary Γ (see figure 4).

We emphasize that the simple evaluation of the view factor (27) is due to the particular geometry of the casting ladle; for a general setup this can be a substantial challenge. We refer to [7] and the references therein where the circular projection method (see [2]) is used to deal with complicated geometries arising when sublimation of SiC single crystals is modelled.

3.3 Initial condition

Finally we introduce the initial condition

$$e(r,z,0) = e_0(r,z) \text{ in D}. \tag{31}$$

Then the initial temperature can be computed by

$$T_0(r,z) = \mathrm{H}^{-1}((r,z), e_0(r,z)) \text{ in D}. \tag{32}$$

3.4 Weak formulation

Multiplying (24) by a test function, integrating in the meridian section D and using a Green´s formula we deduce

$$\int_{\mathrm{D}} \frac{\partial e}{\partial t} v r dr dz + \int_{\mathrm{D}} k \nabla T . \nabla v \; r dr dz = \int_{\partial \mathrm{D}} k \frac{\partial T}{\partial \mathbf{n}} v r d\gamma. \tag{33}$$

Taking into account boundary conditions (8), (9), (21) and (23) this equation reads

$$\begin{aligned} \int_{\mathrm{D}} \frac{\partial e}{\partial t} v \, r \, dr dz + \int_{\mathrm{D}} k \nabla T . \nabla v \, r \, dr dz + \int_{\gamma} \mathcal{G}(\sigma T^4) v r d\gamma = \\ = \int_{\gamma_c} \alpha (T_c - T) v r d\gamma + \int_{\gamma_1} g(\tilde{T}, t) v r d\gamma, \end{aligned} \tag{34}$$

for all test function v.

4 Numerical solution

In this section we use a one-step implicit scheme for time discretization of equation (34) and a finite element method for space discretization. Function T is approximated by piecewise linear finite elements on a triangular mesh.

4.1 Time discretization

We consider the time interval $[0, \mathcal{T}]$, $N \in \mathbb{N}$, $N > 0$ and we set $\Delta t = \mathcal{T}/N$. Now we introduce the mesh $\Pi = \{t^0, \cdots, t^N\}$ of the time interval given by

$$t^0 = 0,$$

$$t^{n+1} = t^n + \Delta t, \;\; n = 0, 1, \ldots N-1.$$

We denote by $F^n(r, z)$ the value of field F at point $(r, z) \in D$ and time $t = t^n$. Now the value of $\dot{e}((r, z), t)$ at $(r, z) \in D$ and $t = t^{n+1}$ is approximated by Euler scheme:

$$\dot{e}((r, z), t^{n+1}) \approx \frac{e^{n+1}(r, z) - e^n(r, z)}{\Delta t}.$$

Therefore, from (34) we obtain **the semi-discretized problem**:

For each $n = 0, 1, \cdots, N-1$ find functions T^{n+1} and e^{n+1} such that

$$\frac{1}{\Delta t}\int_{\mathrm{D}} e^{n+1} v\, r\, dr dz + \int_{\mathrm{D}} k(T^{n+1})\nabla T^{n+1}.\nabla v\, r\, dr dz + \int_{\gamma} \mathcal{G}(\sigma (T^{n+1})^4) v r d\gamma =$$
$$\int_{\gamma_c} \alpha(T_c - T^{n+1}) v r d\gamma + \int_{\gamma_1} g(\tilde{T}^{n+1}, t^{n+1}) v r d\gamma + \frac{1}{\Delta t}\int_{\mathrm{D}} e^n v\, r\, dr dz, \tag{35}$$

for all test function v, where

$$\tilde{T}^{n+1} = \max_{\mathbf{x}\in\gamma_1} T^{n+1}(\mathbf{x}), \tag{36}$$

and

$$e^{n+1}(r,z) \in H((r,z), T^{n+1}(r,z)). \tag{37}$$

4.2 Space discretization

Associated with a family of triangular meshes τ_h of domain D, we consider the space of continuous piecewise linear finite element given by

$$V_h = \{v_h \in \mathcal{C}(\bar{\mathrm{D}}), v_h|_K \in P_1(K)\ \forall K \in \tau_h\}, \tag{38}$$

$P_1(K)$ being the space of polynomials of degree ≤ 1 defined on an element K.

Then we introduce **the discretized problem**:
For each $n = 0, 1, \cdots, N-1$ find the functions T_h^{n+1} and e_h^{n+1} in V_h such that

$$\frac{1}{\Delta t}\int_{\mathrm{D}} e_h^{n+1} v_h\, r\, dr dz + \int_{\mathrm{D}} k(T_h^{n+1})\nabla T_h^{n+1}.\nabla v_h\, r\, dr dz + \int_{\gamma} \mathcal{G}(\sigma (T_h^{n+1})^4) v_h r d\gamma =$$
$$\int_{\gamma_c} \alpha(T_c - T_h^{n+1}) v_h r d\gamma + \int_{\gamma_1} g(\tilde{T}_h^{n+1}, t^{n+1}) v_h r d\gamma + \frac{1}{\Delta t}\int_{\mathrm{D}} e_h^n v_h\, r\, dr dz,\ \forall v_h \in V_h, \tag{39}$$

where

$$\tilde{T}_h^{n+1} = \max_{\mathbf{x}\in\gamma_1} T_h^{n+1}(\mathbf{x}), \tag{40}$$

$$e_h^{n+1}(q) \in H(q, T_h^{n+1}(q)), \tag{41}$$

for all vertices q in $\bar{\mathrm{D}}$.

Notice that the multivalued function H relates temperature to enthalpy; to deal with this nonlinearity, we use an iterative algorithm introduced in Bermúdez & Moreno (see [1]) which is based on the following result:

LEMMA 4.1 *Let H be a maximal monotone operator. The following statements are equivalent:*

i) $p \in H(s) - \omega s$
ii) $p = H_\lambda^\omega(s + \lambda p),\ \lambda > 0,$

where ω and λ are parameters such that $\lambda\,\omega \leq 1/2$ and $\mathrm{H}_\lambda^\omega$ is the Yosida approximation of the operator $H - \omega I$., i.e.

$$H_\lambda^\omega(s) = \frac{[I - ((1-\lambda\omega)I + \lambda H)^{-1}](s)}{\lambda}, \quad s \in \mathbb{R}.$$

At time step $n+1$, we define the function p_h^{n+1} at each vertex q as follows

$$p_h^{n+1}(q) = e_h^{n+1}(q) - \omega T_h^{n+1}(q). \tag{42}$$

From (41) we deduce

$$p_h^{n+1}(q) \in H(q, T_h^{n+1}(q)) - \omega T_h^{n+1}(q),$$

and lemma 4.1 leads to

$$p_h^{n+1}(q) = H_\lambda^\omega(q, T_h^{n+1}(q) + \lambda p_h^{n+1}(q)),\ \ 0 < \lambda \leq \frac{1}{2\omega}. \tag{43}$$

In order to numerically solve (39) the key idea is to replace e_h^{n+1} by $p_h^{n+1} + \omega T_h^{n+1}$ obtaining

$$\frac{\omega}{\Delta t}\int_{\mathrm{D}} T_h^{n+1} v_h\, r\, drdz + \int_{\mathrm{D}} k(T_h^{n+1})\nabla T_h^{n+1}.\nabla v_h\, r\, drdz + \int_{\gamma} \mathcal{G}(\sigma(T_h^{n+1})^4) v_h r d\gamma =$$
$$\int_{\gamma_c} \alpha(T_c - T_h^{n+1}) v_h r d\gamma + \int_{\gamma_1} g(\tilde{T}_h^{n+1}, t^{n+1}) v_h r d\gamma + \frac{1}{\Delta t}\int_{\mathrm{D}} (e_h^n - p_h^{n+1}) v_h\, r\, drdz, \tag{44}$$

for all $v_h \in V_h$, where $\tilde{T}_h^{n+1}$ and p_h^{n+1} are given by (40) and (43), respectively.

4.2.1 Conservation of energy

Equation (39) verifies a discretized equality of conservation of energy. Indeed, multiplying (39) by Δt and taking $v_h = 1$ as a test function we get

$$\int_{\mathrm{D}} e_h^{n+1}\, r\, drdz + \Delta t \int_{\gamma} \mathcal{G}(\sigma(T_h^{n+1})^4) r d\gamma = \Delta t \int_{\gamma_c} \alpha(T_c - T_h^{n+1}) r d\gamma + \Delta t \int_{\gamma_1} g(\tilde{T}_h^{n+1}, t^{n+1}) r d\gamma + \int_{\mathrm{D}} e_h^n\, r\, drdz.$$

Summing these equalities for $n = 0, \cdots, N-1$ we obtain

$$\int_{\mathrm{D}} e_h^{N}\, r\, drdz + \Delta t \sum_{n=0}^{N-1} \int_{\gamma} \mathcal{G}(\sigma(T_h^{n+1})^4) r d\gamma = \Delta t \sum_{n=0}^{N-1} \int_{\gamma_c} \alpha(T_c - T_h^{n+1}) r d\gamma + \Delta t \sum_{n=0}^{N-1} \int_{\gamma_1} g(\tilde{T}_h^{n+1}, t^{n+1}) r d\gamma + \int_{\mathrm{D}} e_h^0\, r\, drdz. \tag{45}$$

Using (26) in the integral of the second term of (45) we get

$$I = \int_{\gamma}\int_{\gamma} \sigma f(r,z,\tilde{r},\tilde{z}) \left[(T_h^{n+1})^4(r,z) - (T_h^{n+1})^4(\tilde{r},\tilde{z})\right] \tilde{r}\; d\gamma_{(\tilde{r},\tilde{z})} r\, d\gamma_{(r,z)},$$

then

$$I = \int_{\gamma}\int_{\gamma} \sigma f(r,z,\tilde{r},\tilde{z})\, (T_h^{n+1})^4(r,z)\; \tilde{r}\; d\gamma_{(\tilde{r},\tilde{z})}\, r\, d\gamma_{(r,z)} - - \int_{\gamma}\int_{\gamma} \sigma f(r,z,\tilde{r},\tilde{z})\, (T_h^{n+1})^4(\tilde{r},\tilde{z})\, \tilde{r}\; d\gamma_{(\tilde{r},\tilde{z})} r\, d\gamma_{(r,z)}.$$

Interchanging the order of integration in the first integral we get

$$I = \int_{\gamma}\int_{\gamma} \sigma f(r,z,\tilde{r},\tilde{z})\, (T_h^{n+1})^4(r,z)\, r\; d\gamma_{(r,z)} \tilde{r}\; d\gamma_{(\tilde{r},\tilde{z})}\; - - \int_{\gamma}\int_{\gamma} \sigma f(r,z,\tilde{r},\tilde{z})\, (T_h^{n+1})^4(\tilde{r},\tilde{z})\, \tilde{r}\; d\gamma_{(\tilde{r},\tilde{z})} r\, d\gamma_{(r,z)}.$$

Finally, using (28) we deduce

$$I = \int_{\gamma}\int_{\gamma} \sigma f(\tilde{r},\tilde{z},r,z)\, (T_h^{n+1})^4(r,z)\, r\; d\gamma_{(r,z)} \tilde{r}\; d\gamma_{(\tilde{r},\tilde{z})}\; - - \int_{\gamma}\int_{\gamma} \sigma f(r,z,\tilde{r},\tilde{z})\, (T_h^{n+1})^4(\tilde{r},\tilde{z})\, \tilde{r}\; d\gamma_{(\tilde{r},\tilde{z})} r\, d\gamma_{(r,z)},$$

and conclude that I equals zero. Thus (45) reads

$$\int_{\mathrm{D}} (e_h^N - e_h^0)\, r\, dr dz = \Delta t \sum_{n=0}^{N-1} \int_{\gamma_c} \alpha(T_c - T_h^{n+1}) r d\gamma + \Delta t \sum_{n=0}^{N-1} \int_{\gamma_1} g(\tilde{T}_h^{n+1}, t^{n+1}) r d\gamma, \tag{46}$$

which shows that energy is conserved by the scheme.

REMARK 4.1 As we mention below, the integrals appearing in the weak formulation (39) have to be approximated by using quadrature formulas. Fortunately, analogous computations to those we have made above show that equality (46) also holds with the integrals replaced with these quadrature formulas, in which case it can be viewed as an energy conservation principle for the fully approximate scheme.

4.3 An iterative algorithm

In this section we present an iterative algorithm consisting of three embedded loops as the flow chart of the algorithm shows in figure 7. Hereafter we omit subscript h associated with the space discretization for the sake of simplicity.

Initial time step: e_0 is given and T_0 is computed using (32). Therefore $T^0 = T_0$ and $p^0 = e_0 - \omega\, T^0$.

1.- Time loop:

Let us suppose that T^n and p^n are known. Then $e^n = \omega\, T^n + p^n$. At time t^{n+1}, function T^{n+1} is obtained as the limit of the sequence T_s^{n+1} coming from the following iterative algorithm:

2.- Nonlinear loop

(a) Initialization: for $n \geq 0$, $T_0^{n+1} = T^n$ and $p_0^{n+1} = p^n$.

(b) $(s+1)$**-th iteration:** T_s^{n+1} and p_s^{n+1} are known. Function T_{s+1}^{n+1} is obtained as the limit of the sequence $T_{s+1,k}^{n+1}$ computed by

3.- Multiplier loop

(i) Initialization: $T_{s+1,0}^{n+1} = T_s^{n+1}$ and $p_{s+1,0}^{n+1} = p_s^{n+1}$.

(ii) $(k+1)$**-th iteration**: $p_{s+1,k}^{n+1}$ is known and in order to compute

$T^{n+1}_{s+1,k+1}$ and $p^{n+1}_{s+1,k+1}$ we proceed as follows:

- $T^{n+1}_{s+1,k+1}$ is the solution of the linear problem

$$\frac{\omega}{\Delta t}\int_{\mathrm{D}} T^{n+1}_{s+1,k+1} v\, r\, drdz + \int_{\mathrm{D}} k(T^{n+1}_{s})\nabla T^{n+1}_{s+1,k+1}.\nabla v\, r\, drdz + \int_{\gamma} \mathcal{G}(\sigma(T^{n+1}_{s})^4) v\, r\, d\gamma = \int_{\gamma_c} \alpha(T_c - T^{n+1}_{s+1,k+1}) v\, r\, d\gamma + \int_{\gamma_1} g(\tilde{T}^{n+1}_{s}, t^{n+1}) v\, r\, d\gamma + \frac{1}{\Delta t}\int_{\mathrm{D}} (e^n - p^{n+1}_{s+1,k}) v\, r\, drdz, \tag{47}$$

  for all $v \in V_h$ where

$$\tilde{T}^{n+1}_{s}(\mathbf{x}) = \max_{\mathbf{x}\in\gamma_1} T^{n+1}_{s}(\mathbf{x}) \tag{48}$$

- Then $p^{n+1}_{s+1,k+1}$ is calculated at every vertex q of the mesh using the formula

$$p^{n+1}_{s+1,k+1}(q) = \mathrm{H}^{\omega}_{\lambda}(q, T^{n+1}_{s+1,k+1}(q) + \lambda p^{n+1}_{s+1,k}(q)). \tag{49}$$

A two-point Gaussian quadrature on each edge of the boundary is employed to integrate the boundary terms in (47). The use of this quadrature determines that equality (19) can only be obtained approximately. Actually, we have computed the relative errors by using both the trapezoidal rule and the above mentioned two-point Gaussian formula. For the mesh shown in figure 8, they are 5% and 0.5%, respectively.

REMARK 4.2 Choleski factorization has been employed to solve the linear system arising from (47). Notice that the matrix of this system is not modified in the innermost loop of this algorithm.

Theoretical results concerning the convergence of algorithm (47)-(49) without the radiation term can be found in [1] using maximal monotone operator techniques. To our knowledge, the analysis of convergence considering the radiative contribution is an open problem.

For $\Delta t = 1s$ and the mesh shown in figure 8, the average number of iterations per time step are 1.1 for the outer nonlinear loop and 25 for the inner multiplier loop. If the radiation term is omitted in (47), these average numbers are 1 and 22, respectively. Therefore, we can conclude that the phase change is the main nonlinearity and the presence of the radiation term does not increase significantly the algorithmic difficulty of the problem.

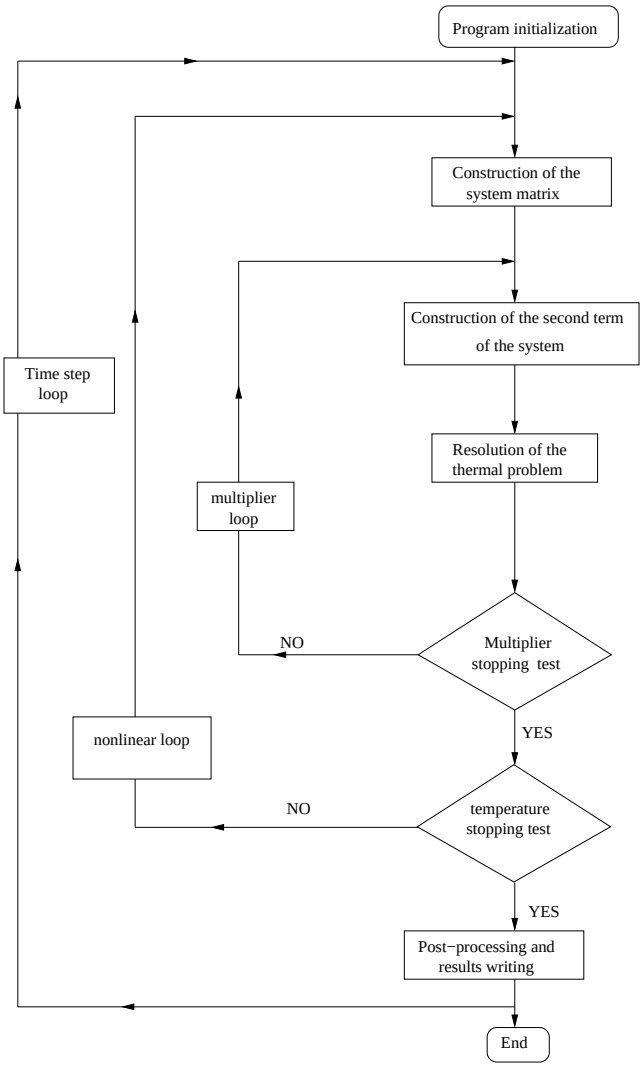

Fig. 7. Flow chart of the algorithm.

REMARK 4.3 From the stability point of view, there is no problem in treating the radiation term explicitly in time. This has been done in our code with $\mathcal{T} = 1000\,s$ and we have not observed any instability problem. Moreover, the L^2-norm of the difference between the solution for time-implicit and time-explicit radiation term is only $4.45 \times 10^{-4}\%$.

5 Numerical results

The aforementioned algorithm has been implemented in a computer code written in Fortran and in this section we present several numerical results concerning this code. The computation was performed on a personal computer working under Windows.

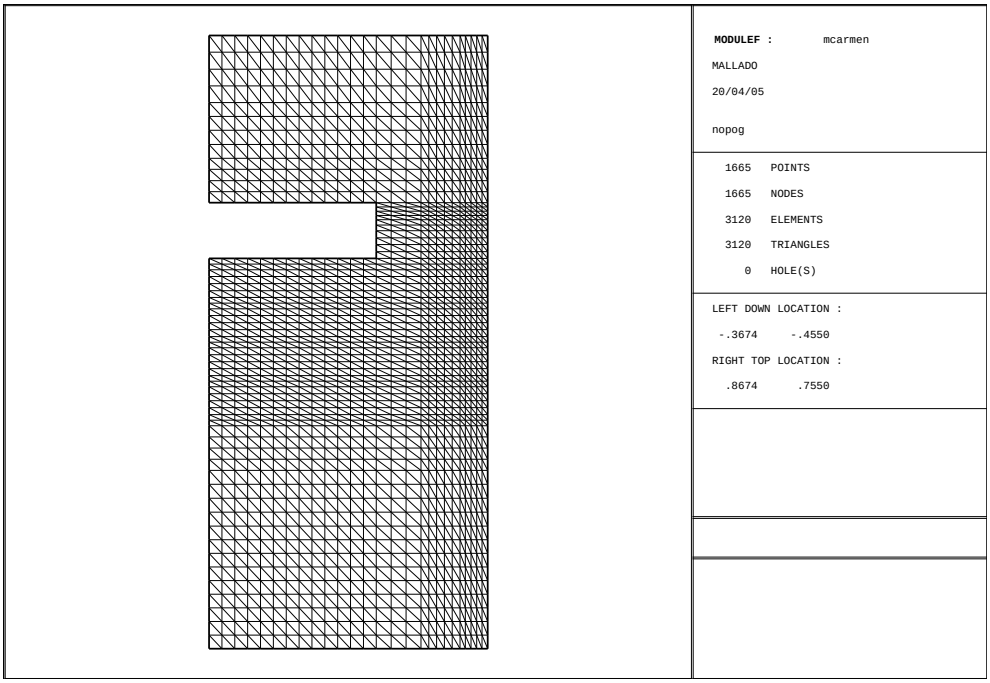

Fig. 8. Geometry and mesh of the ladle with silicon.

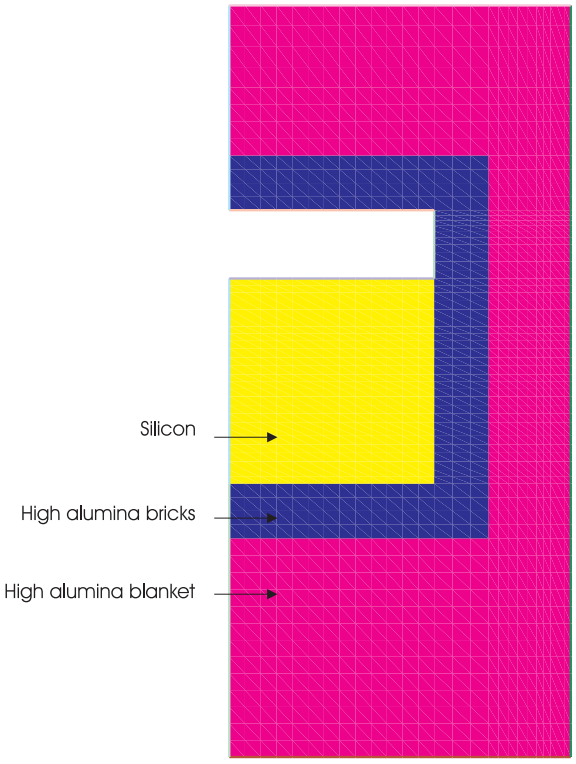

Fig. 9. Materials of the ladle with silicon.

Figure 8 shows the geometry and the mesh used for finite element discretization. It was made with Modulef library (see [12]). Figure 9 presents the configuration of the materials forming the ladle.

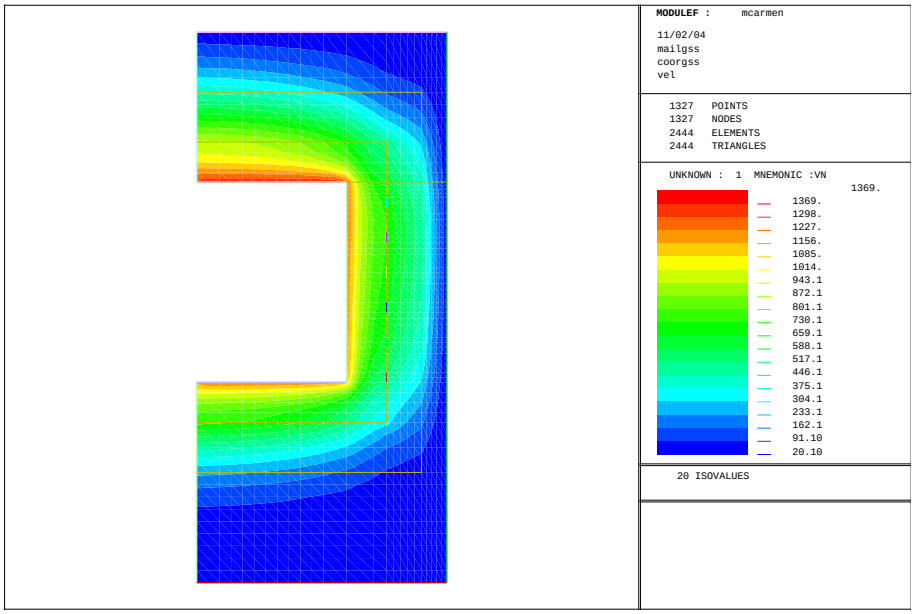

Fig. 10. Isotherms (°C) of the preheated ladle.

The ladle is preheated using the inner heating elements. Isotherms of the preheated ladle are shown in figure 10. Notice the distribution of heat at the inner walls of the ladle due to the non-local radiation condition: the heat generated on γ_1 is almost uniformly distributed on the walls of the enclosure. Then, silicon at 1480 °C is poured into the inner cavity. The power of the heating elements is 10 kW during the first 40000 s; afterwards, the power is decreasing to zero as time increases, i.e., function $p(t)$ of (11) is given by

$$p(t) = \begin{cases} 10 \text{ kW} & \text{if } t \leq 40000\, s, \\ \dfrac{10}{(t - 39999)^{1/5}} \text{ kW} & \text{if } t > 40000\, s. \end{cases} \tag{50}$$

Moreover, $\underline{\theta} = 1450\,°\text{C}$ and $\bar{\theta} = 1550\,°\text{C}$.

Figures 11 and 12 show the solidification front corresponding to times $t = 1000\, s$ and $t = 36000\, s$, respectively. We remark that silicon solidifies around the walls of the inner enclosure at the beginning of the process, and then the solidification front is progressively getting flatter.

With figure 13, showing the solidification front at time $t = 128000\, s$, we emphasize the fact that the solidification front grows upwards as time increases; thus the top of the silicon ingot is the last part to solidify.

Acknowledgements

Authors thank the engineers of FERROATLANTICA I+D (A Coruña, Spain), in special J. Bullón, for their collaboration in this work. We also thank F.

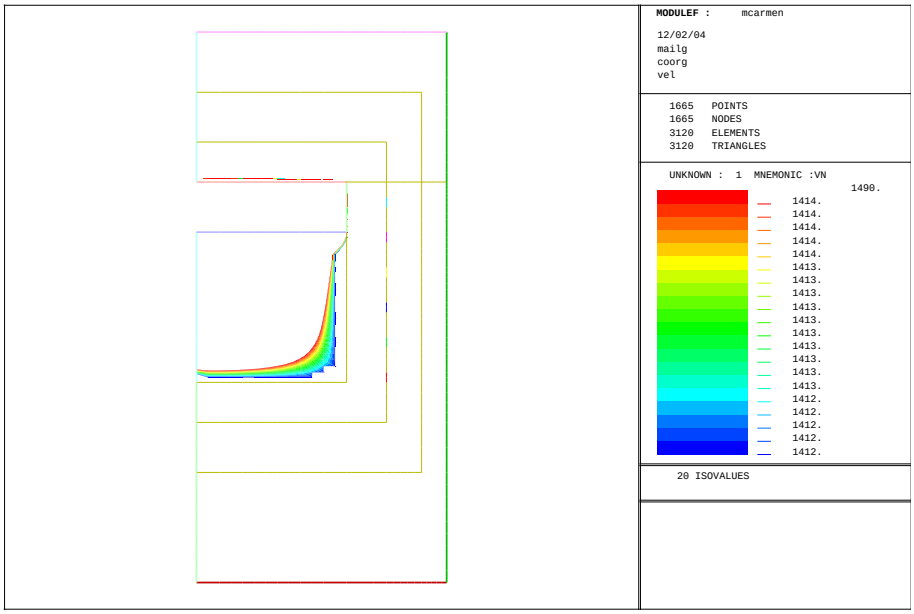

Fig. 11. Solidification front at $t = 1000\,s$.

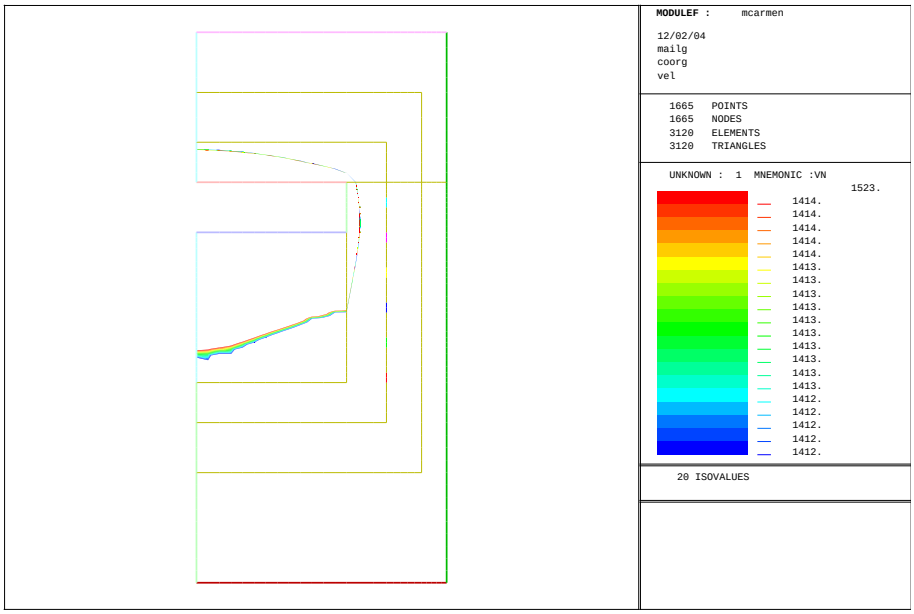

Fig. 12. Solidification front at $t = 36000\,s$.

Guitián, V. Valcárcel, J.L. Ferrín and O. López from University of Santiago de Compostela for some valuable suggestions. Authors are indebted to the referees for their helpful remarks.

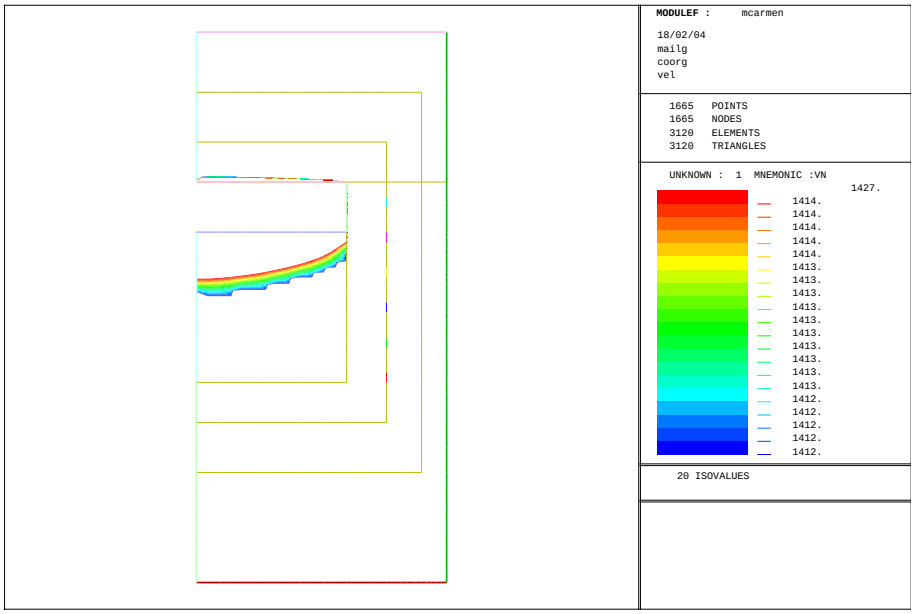

Fig. 13. Solidification front at $t = 128000\,s$.

List of symbols

$\mathbf{x}$	spatial variable
t	time
T	temperature
ρ	density
c	specific heat
k	thermal conductivity
H	enthalpy function
L	latent heat
T_s	temperature of silicon phase change
e	enthalpy density
α	convective heat transfer coefficient
T_c	temperature of surroundings
g	function representing the power given to heating elements
J	irradiation
R	radiosity
σ	Stefan-Boltzmann constant
F	view factor
T_0	initial condition
$\mathcal{T}$	final time
N	number of time subintervals
Δt	time discretization step
H_λ^ω	Yosida approximation

References

[1] Bermúdez, A. & Moreno, C., Duality methods for solving variational inequalities. Comput. Math. Appl., 7 (1981), 43–58.

[2] Dupret, F., Nicodème, P., Ryckmans, Y., Wouters, P. & Crochet, M.J. Global modelling of heat transfer in crystal growth furnaces. Int. J. Heat Mass Transfer, 33 (1990) 1849–1871.

[3] Ern, A. & Guermond, J.L. Accurate numerical simulation of radiative heat transfer with application to crystal growth. Int. J. Numer. Meth. Engng, 61 (2004) 559–583.

[4] Hlaváček, I. & Křížek, M., Dual finite element analysis of three-dimensional axisymmetric elliptic problems. Part I. Numerical Methods for Partial Differential Equations, 9 (1993), 507–526.

[5] Hsu, P. F. & Ku ,J. C., Radiative heat transfer in finite cylindrical enclosures with nonhomogeneous participating media. Journal of Thermophysics and Heat Transfer, 8(3) (1994), 434–440.

[6] Incropera, F. P. & De Witt ,D. P., *Fundamentals of heat and mass transfer*, Wiley, (New York, 1990).

[7] Klein,O., Philip, P., Sprekels, J. & Wilmański, K., Radiation- and convection-driven transient heat transfer during sublimation growth of silicon carbide single crystals. Journal of Crystal Growth, 222 (2001) 832–851.

[8] Metzger, M., Existence for a time-dependent heat equation with non-local radiation terms. Math. Meth. Appl. Sci., 22 (1999), 1101–1119.

[9] Nunes, E. M., Modi, V. & Naraghi, M. H. N., Radiative transfer in arbitrarily-shaped axisymmetric enclosures with anisotropic scattering media. International Journal of Heat and Mass Transfer, 43 (2000), 3275–3285.

[10] Nunes, E. M. & Naraghi,M.H.N., Numerical model for radiative heat transfer analysis in arbitrarily shaped axisymmetric enclosures with gaseous media. Numerical Heat Transfer, Part A, 33 (1998), 495–513.

[11] Tiihonen, T., Stefan-Boltzmann radiation on non-convex surfaces, Mathematical Methods in the Applied Sciences, 20 (1997), 47–57.

[12] Toit, H. D., *Introduction à MODULEF. Guide #1*, INRIA, (France, 1991).

[13] Zeidler, E., *Nonlinear functional analysis and its applications, II/B Nonlinear monotone operators*, Springer-Verlag, (New York, 1990).